A Simplified Coupled Model of Extended-Range Predictability

ARTHUR J. MILLER AND JOHN O. ROADS

Climate Research Division, Scripps Institution of Oceanography, La Jolla, California

(Manuscript received 23 June 1989, in final form 30 October 1989)

ABSTRACT

A simplified coupled atmosphere–ocean model is used to explore the influence of evolving midlatitude sea surface temperature (SST) anomalies on the theoretical extended-range predictability of the atmospheric wintertime circulation in the Northern Hemisphere. After approximately two weeks, SST anomalies begin to significantly influence the overlying atmospheric flow, compared to flow over the climatological SST field. If the evolving sea surface temperature field is specified from model "observed" flows, then predictions of atmospheric time-averaged flow, for one month and longer averages, are significantly enhanced over predictions based on the atmospheric model with climatological SST. Predictions using the coupled model, however, are not significantly different from predictions using the atmospheric model with persistent SST anomalies, because SST anomalies are forced increasingly erroneously by atmospheric variables that rapidly lose their predictability.

1. Introduction

Extended-range (weeks to a season) dynamical hindcasts of observed atmospheric features are often improved by including observed sea surface temperature (SST, hereinafter) anomalies, especially those associated with strong tropical warming (WMO 1988, and references therein). The impact of midlatitude SST anomalies on numerical simulations of the overlying atmospheric flow is more subtle but it appears to be significant (Palmer and Zhaobo 1985; Pitcher et al. 1988), and such anomalies have been a longstanding candidate for improving empirical and statistical seasonal forecasts of extra-tropical circulation (e.g., Namias 1976; Davis 1978).

It remains unclear, however, whether extended-range hindcasts of the atmosphere are significantly improved when typical midlatitude SST anomalies are specified from observations as boundary conditions. Indeed, even if observed SST is shown to influence hindcasts of the atmosphere its usefulness in the forecasting problem is still moot. For it is unclear whether midlatitude SST can be dynamically predicted with sufficiently greater skill than a forecast of SST persistence to justify the expense of its dynamical prediction as a boundary condition for the atmospheric forecast model. This is because the atmospheric variability, which is the dominant forcing function of the midlatitude SST anomalies (Frankignoul and Reynolds 1983), must be simultaneously predicted.

Towards understanding the theoretical usefulness of coupled models in extended-range prediction, we use herein a simplified coupled atmosphere–ocean model of the Northern Hemispheric January circulation to explore the influence of evolving midlatitude SST anomalies on the extended-range predictability of the atmosphere and ocean. The two-layer atmosphere (Roads 1987a,b, 1989b) is quasi-geostrophic, with orography and time-dependent forcing by variable sea and land-surface temperature. The SST variability is modeled by a slab mixed-layer model that is influenced by atmospheric heat flux and, in the North Pacific Ocean, additionally by Ekman-current advection and geostrophic-current advection. The simplified dynamics not only allow us to obtain large ensembles of predictions, which then provide measures of statistical reliability, but also enable us to explore different physical mechanisms of SST anomaly generation.

After we generate a base run of the coupled system, which is taken to represent "observed" flows, we implement various prediction models to determine their relative success at dynamical prediction. The prediction models, initialized with small-scale error, use the same atmospheric model with different ocean models:

(i) SST fixed at climatic values (climatic SST)
(ii) SST fixed at anomalous initial values (persistent SST)
(iii) SST predicted by coupled dynamics (predicted SST)
(iv) SST specified from base run (true SST)

We are then able to address the following questions concerning the importance of midlatitude SST in extended-range forecasting. On what time scale does

Corresponding author address: Dr. Arthur J. Miller, Climate Research Division, A-024, Scripps Institution of Oceanography, University of California, San Diego, La Jolla, CA 92093.

anomalous SST influence the overlying atmospheric flow? Is a coupled model more skillful in dynamical prediction than an uncoupled atmosphere with a persistent initial SST anomaly as a boundary condition? If midlatitude SST is specified from observations as a boundary condition, how much improvement should we expect in hindcasts of atmospheric variability? How well can we expect to be able to predict SST given even a "perfect" SST model, since the forcing function (the atmosphere) must be predicted as well?

Section 2 describes the dynamics of the coupled model used for these investigations. The climatology of the coupled system is discussed in section 3 and the predictability results are detailed in section 4. Preliminary answers to the above questions, as deduced from our simplified coupled model, are given in section 5, which also includes a summary and several caveats on the interpretation of these results.

2. Summary of the coupled atmosphere–ocean models

During the course of this study, we examined results from five different coupled scenarios, three for which predictability experiments were systematically executed. The only differences between cases, outlined in Table 1 and discussed more completely in section 3, were in the distribution of the surface heat-exchange coefficient, K_g, and in the mechanisms for SST variability at Pacific Ocean gridpoints. In this section, the coupled model framework is summarized. Somewhat similar coupled systems have been considered by Pedlosky (1975) and Salmon and Hendershott (1976).

a. *Model dynamics*

The atmospheric model, discussed in detail by Roads (1987a,b; 1989b), is a two-level, Northern Hemispheric, quasi-geostrophic, nonlinear, time-dependent system. The nondimensional equations are

$$\frac{\partial}{\partial t} q_1 + J(\psi_1, q_1) + K\nabla^6\psi_1 - 2\lambda^2(K_T + K_R)\tau = F_B - F_T - 2\lambda^2 K_T \alpha T_m \quad (2.1)$$

$$\frac{\partial}{\partial t} q_3 + J(\psi_3, q_3) + K\nabla^6\psi_3 + K_s\nabla^2\psi_3 + 2\lambda^2(K_T + K_R)\tau = F_B + F_T + 2\lambda^2 K_T \alpha T_m. \quad (2.2)$$

TABLE 1. Differences between coupled simulations.

Case	Pacific SST forcing	Heat-transfer field, K_g
A	Heat flux alone	Fig. 1a
B	Currents alone	Fig. 1a
C	Currents alone	Fig. 1b
D	Currents and heat flux together	Fig. 1b
E	Heat flux alone	Fig. 1b

Here ψ_1 is the upper-level streamfunction, ψ_3 is the lower-level streamfunction, $\tau = (\psi_1 - \psi_3)/2$ is the baroclinic (thermal) streamfunction, $q_i = \nabla^2\psi_i \mp 2\lambda^2\tau + \sin(\theta) + h$ is the potential vorticity for level i, F_B and F_T are the barotropic and thermal components of the forcing, respectively, T_m is the land or ocean surface temperature, $K = 3 \times 10^{-7}$, $K_T = 1.5 \times 10^{-2}$, $K_R = 3 \times 10^{-3}$, $K_s = 3 \times 10^{-2}$, $\lambda^2 = 50$, $\alpha = 2.4 \times 10^{-4}$ and all the variables and parameters are nondimensionalized with 2Ω and the radius of the earth.

The effects of parameter choices on the mean circulation are minimized by the calculation of the steady forcing using a residual method. That is, given the observed fields $\tilde{\psi}_1$, $\tilde{\psi}_3$, and $\tilde{T}_m$, for each January day of the ten Januaries available for this study, it is possible to derive F_T and F_B roughly compatible with such observations. More precisely,

$$F_B = \frac{1}{2}\{J(\tilde{\psi}_1, \tilde{q}_1) + J(\tilde{\psi}_3, \tilde{q}_3) + K\nabla^6(\tilde{\psi}_1 + \tilde{\psi}_3) + K_s\nabla^2\tilde{\psi}_3\}, \quad (2.3)$$

$$F_T = \frac{1}{2}\{J(\tilde{\psi}_3, \tilde{q}_3) - J(\tilde{\psi}_1, \tilde{q}_1) - 2K\nabla^6\tilde{\tau} + 4\lambda^2(K_T + K_R)\tilde{\tau} + K_s\nabla^2\tilde{\psi}_3 - 4\lambda^2 K_T \alpha \tilde{T}_m\} \quad (2.4)$$

where $\{\cdot\}$ denotes a time average over the 10-year sequence of daily observed fields.

Roads (1987a, 1989b) has extensively discussed the model atmosphere's ability to simulate observed aspects of the general circulation including the energy cycle. Horel and Roads (1988) show that the model exhibits quasi-stationary regimes with frequency of occurrence and characteristics similar to those observed. With the F_T and F_B of (2.3) and (2.4), the atmospheric model climatology is similar in many respects to the observed January climatology, both in stationary features and transient variations. The relative magnitude of the atmospheric model's intrinsic predictability decay time and the response time to SST anomaly forcing is important in determining the impact of SST anomalies on the predictability of the atmosphere. Roads (1987a) showed that the atmospheric model's predictability decay time scale (rms error doubling time $\approx$ 3 days) is comparable to those of present numerical weather prediction models. The choice of K_T sets the time scale of atmospheric response to SST anomalies, which is poorly known, particularly in midlatitudes. Roads (1989b), however, discussed the atmospheric model's response to fixed SST anomalies and showed that, with $K_T = (5.3 \text{ day})^{-1}$, the model atmospheric response is comparable to the NCAR GCM response to similar fixed SST anomalies (Pitcher et al. 1988). In particular, the atmospheric model's response is equivalent barotropic, the amplitude of the atmospheric thermal response is approximately equal to that of the SST anomaly and the atmosphere develops a dipole-like pattern above the SST anomaly with the strongest re-

sponses at the upper level being about 60 meters over a 1°C SST anomaly. It therefore appears that the atmospheric model is satisfactory for the extended-range predictability studies of our coupled system.

The surface temperature T_m for land and non-Pacific oceans is determined according to

$$\frac{\partial T_m}{\partial t} = K_g(T_a - T_m) + K\nabla^4 T_m + F_m \quad (2.5)$$

where the atmospheric temperature $T_a = (\tau/\alpha)$ and K_g is shown in Fig. 1. For Pacific Ocean gridpoints north of 10°N, SST is governed by

$$\frac{\partial T_m}{\partial t} + A\nabla\psi_3 \cdot \nabla T_m + J(\phi_1, T_m) = K_g(T_a - T_m) + \kappa\nabla^2 T_m + F_m. \quad (2.6)$$

The Ekman advection velocity, $A\nabla\psi_3 = \mathbf{k} \times \vec{\tau}/\rho_o f H$, is specified from a scaled version of the wind of the atmospheric lower layer (750 mb flow). The geostrophic advection velocity is specified from the upper-layer streamfunction, ϕ_1, of the quasi-geostrophic ocean model (2.12)–(2.15). The energy balance requirement that the heat transferred to the atmosphere be equivalent to the heat transferred from the ocean implies that

$$\frac{\partial}{\partial t}\left[\frac{P_o c_p}{g} T_a + \rho_o H c_p' K_g T_m\right] = 0 \quad (2.7)$$

and determines the relation between mixed-layer depth and the heat transfer coefficients:

$$K_g = \frac{P_o c_p K_T}{\rho_o g H c_p'} \quad (2.8)$$

where P_o = sea level pressure, c_p = specific heat of the atmosphere, ρ_o = density of sea water, g = gravitational acceleration, c_p' = specific heat of sea water and K_T and K_g are the dimensional heat transfer coefficients. The choice of a constant oceanic mixed-layer depth, H = 50 m, sets the SST decay time scale K_g^{-1} = 58 days. The horizontal diffusion coefficient κ = 500 $m^2\ s^{-1}$.

Since the atmospheric model's fluctuations were deficient compared to observations, we specified wind stress according to

$$\vec{\tau} = c_D \rho_a |U_o| [1.7(\nabla\psi_3 - 0.8\nabla\bar{\psi}_3)] \quad (2.9)$$

where ψ_3 and $\bar{\psi}_3$ are the instantaneous and uncoupled-mean streamfunctions of the lower (750 mb) layer of the model atmosphere. The values $c_D = 1.5 \times 10^{-3}$, ρ_a = 1.25 kg m^{-3} and $|U_o|$ = 16.4 m s^{-1} then yield both mean and fluctuating wind stresses which are comparable to observations (Figs. 2a,b).

In order to maintain a realistic distribution of time-averaged SST, we specify F_m in a similar fashion as in (2.3) and (2.4). For non-Pacific regions,

$$F_m \equiv \{K\nabla^4 T_m - K_g(T_a - T_m)\}. \quad (2.10)$$

For the Pacific region,

$$F_m \equiv A\nabla\bar{\psi}_3 \cdot \nabla\{T_m\} + J(\bar{\phi}_1, \{T_m\}) - K_g(\bar{T}_a - \{T_m\}) - \kappa\nabla^2\{T_m\} \quad (2.11)$$

where the overbars denote time averages from decoupled integrations of the model atmosphere and ocean and the $\{\cdot\}$ again denotes a time average over 10-years of observations.

The geostrophic velocity in (2.6) is specified by solving a two-layer quasi-geostrophic (QG) ocean model, originally developed by W. R. Holland and J. C. Chow of the National Center for Atmospheric Research, according to

$$\frac{\partial}{\partial t}\nabla^2\phi_1 + J(\phi_1, \nabla^2\phi_1 + f) + \frac{f_o}{H_1} w_2 = \frac{\text{curl}\,\vec{\tau}}{\rho_o H_1} + A\nabla^4\phi_1 + F_1 \quad (2.12)$$

$$\frac{\partial}{\partial t}\nabla^2\phi_3 + J(\phi_3, \nabla^2\phi_3 + f) - \frac{f_o}{H_3} w_2 = -r\nabla^2\phi_3 + A\nabla^4\phi_3 \quad (2.13)$$

where

$$w_2 = \frac{f_o}{g''}\left\{J(\phi_1 - \phi_3, \phi_2) - \frac{\partial}{\partial t}(\phi_1 - \phi_3)\right\} \quad (2.14)$$

$$\phi_2 = \frac{H_1\phi_3 + H_3\phi_1}{H_1 + H_3} \quad (2.15)$$

and where ϕ_i is the velocity streamfunction in layer i, w_2 is the vertical velocity at the interface between the layers, H_i is the mean depth of layer i (1 km and 4 km for layers 1 and 3, respectively), $g'' = g\Delta\rho/\rho_o$ = 0.02 m s^{-2} is the reduced gravity based on the density jump at the main thermocline, A = 1600 $m^2\ s^{-1}$ is the lateral diffusion coefficient, $r = 10^{-7}\ s^{-1}$ is the bottom friction (Ekman drag) coefficient, $f = 2\Omega\sin(\theta)$ is the Coriolis frequency, which allows β to be a function of latitude θ, and $f_o = 8.3 \times 10^{-5}$ is Coriolis frequency at midbasin.

The curl of the atmospheric wind stress, curl$\vec{\tau}$, is tuned as in (2.9) except that the uncoupled-mean curl is completely removed so that

$$\text{curl}\vec{\tau} = c_D\rho_a|U_o|[1.7(\nabla^2\psi_3 - \nabla^2\bar{\psi}_3)]. \quad (2.16)$$

The mean driving of (2.9) is contained in F_1, a residual steady state forcing included to adjust the flow towards a climatologically observed mean, defined by

$$F_1 \equiv J(\hat{\phi}_1, \nabla^2\hat{\phi}_1 + f) \quad (2.17)$$

where $\hat{\phi}_1$ indicates observed wintertime fields of dynamic height at the ocean surface relative to 2000 m depth (Levitus 1982), converted to streamfunction and the remaining notation is standard.

The horizontal geometry for (2.6), (2.12) and (2.13) is discretized on a spherical 1° grid and is patterned after the North Pacific basin, with an artificial boundary

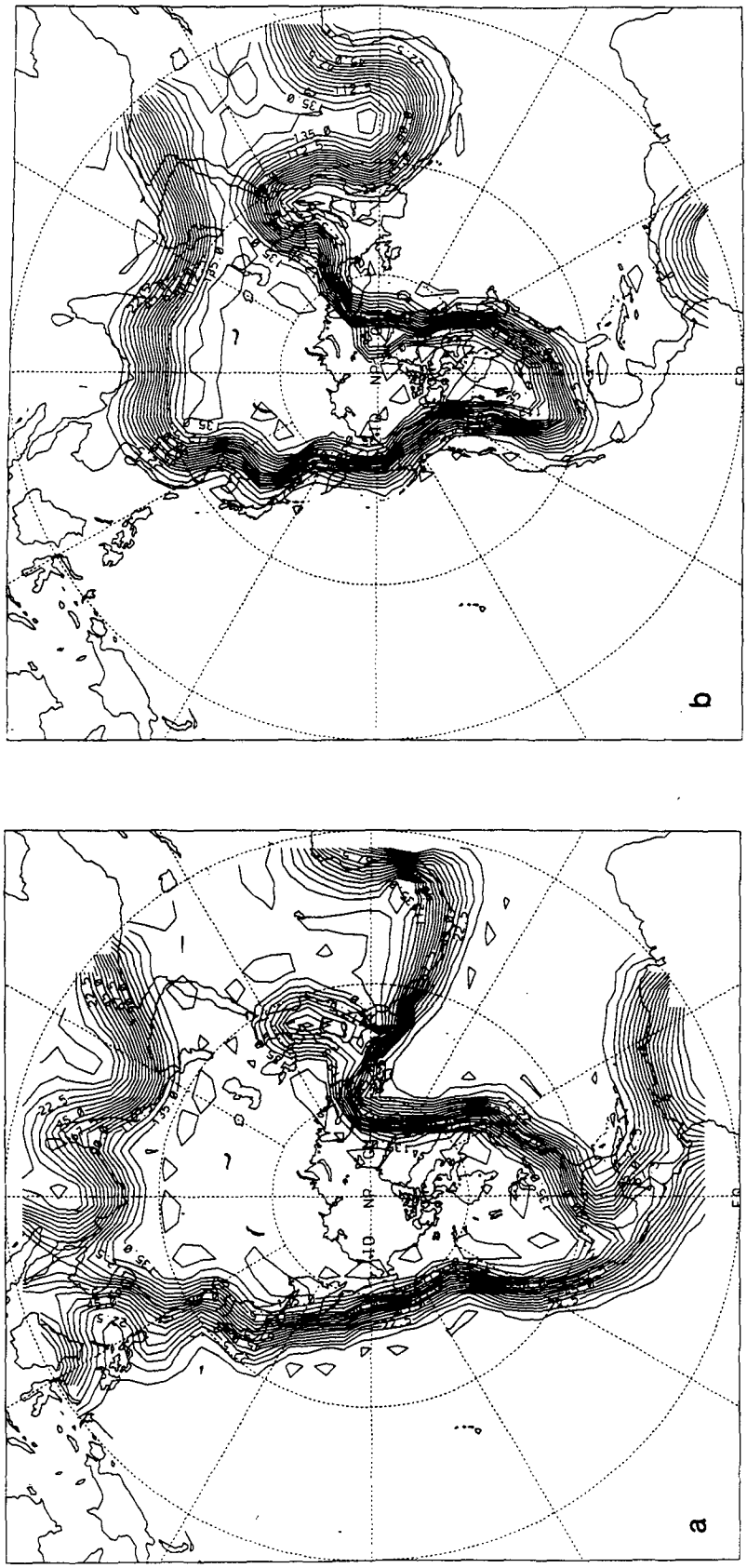

FIG. 1. Hemispheric fields of ground temperature heat exchange coefficient, K_g, for (a) Cases A and B and (b) Cases C, D and E. Ocean values equal 2×10^{-7} day^{-1} and land values equal 2×10^{-5} day^{-1}. Values scaled by 10^7, Contour interval (CI, hereinafter) = 7.5.

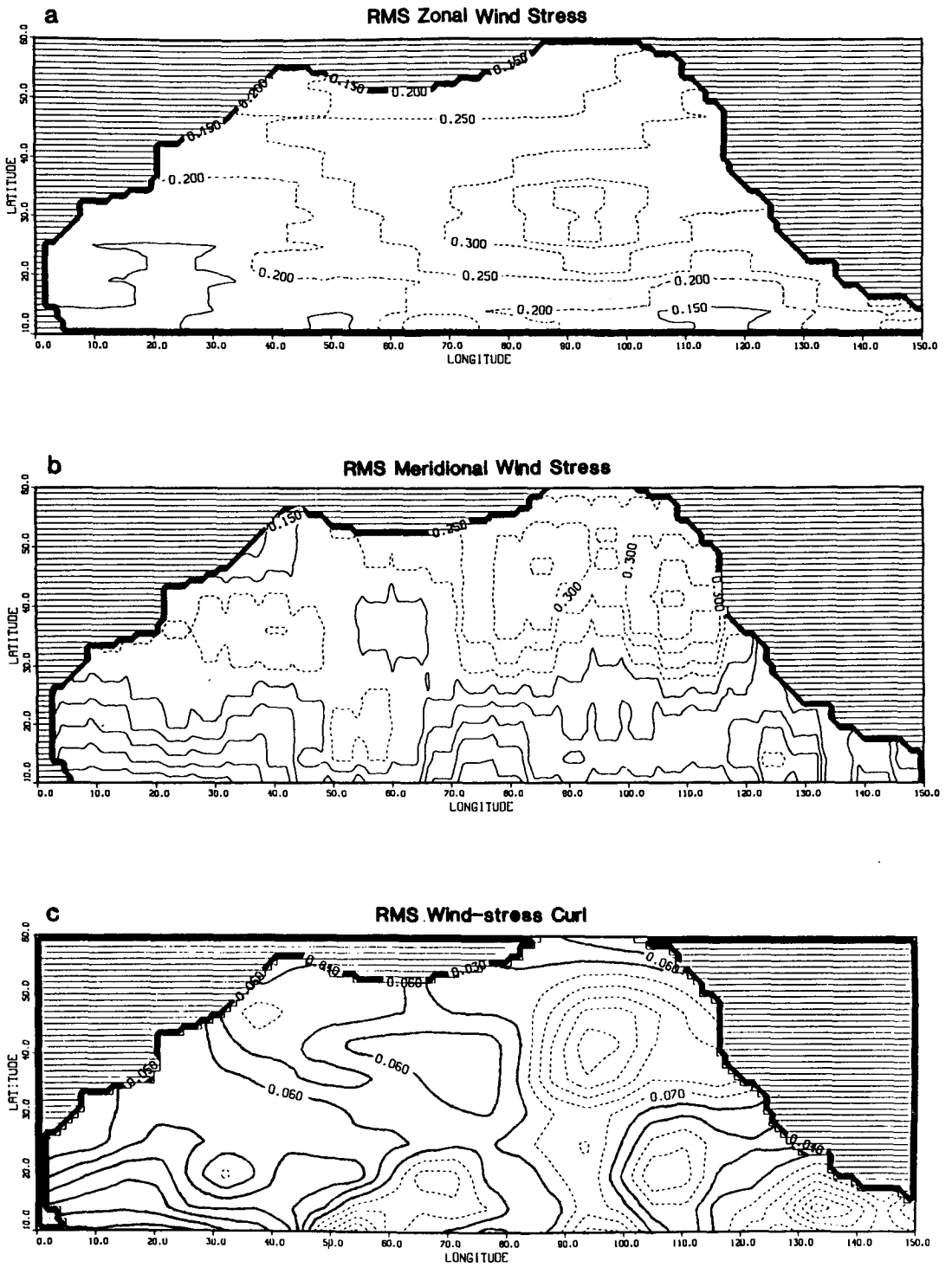

FIG. 2. Standard deviations of (a) zonal wind stress (Nt/m^2, CI = 5×10^{-2}, dashed contours ≥ 0.20), (b) meridional wind stress (Nt/m^2, same contouring as for zonal), and (c) wind-stress curl (Nt/m^3, CI scaled by 7.8×10^{-6}, dashed contours $\geq 3.9 \times 10^{-7}$). Each field is derived from the 1800-day atmospheric model simulation in Case A. The stress fields are dominated by a large-scale pulsating vortex in the northeastern Pacific. Monthly averaged versions of the pictured fields are fairly similar in structure, although the standard deviations are reduced, typically to approximately one-third of the plotted values. Rms meridional (a) and zonal (b) Ekman currents in m s^{-1} are equal to the plotted stresses times 0.24. In all the Pacific basin figures, "longitude" is referenced with respect to 120°W.

imposed along 10°N. Along the boundaries the free-slip condition $\nabla^2\psi_i = 0$ is enforced. The friction is strong enough to extinguish any instabilities in the oceanic QG model.

Various diagnostics of the North Pacific flow patterns, QG model response and SST response characteristics were investigated for simulations in coupled and uncoupled mode, but only a brief discussion of those results is permitted here. Figure 3 shows the rms SST distribution for uncoupled runs when the anomalous heat-flux forcing is shut off ($T_a = \bar{T}_a$) in (2.6). Rms values for SST anomalies generated solely by variability of either geostrophic (Fig. 3a) or Ekman (Fig. 3b) currents are 0.5°C rms, although the spatial scale of the Ekman-driven anomalies is much larger than those due to geostophic-current advection. Figure 4b shows the rms SST distribution when the ocean-current fields are shut off ($\psi_3 = 0$ and $\phi_1 = 0$) in (2.6) and only anomalous heat fluxes from the T_a variability (Fig. 4a) drive the anomalies. Figure 4c shows the rms SST distribution when current-advection and heat fluxes operate together in uncoupled mode. In coupled mode (Fig. 4d), the ocean influences the atmosphere to produce SST variations (reduced relative to the uncoupled case) which are O(1°C), compared to observed standard deviations of monthly averaged Janaury SST which are 0.6°–0.9°C (Cayan 1980) in the Pacific. The coupled model thus appears to be suitable for exploring the impact of SST variablity on the theoretical predictability of the coupled atmosphere–ocean system.

b. *Coupling strategy*

The flow of information between atmosphere, surface temperature, and deep quasi-geostrophic ocean is as follows. The atmosphere forces land-surface temperature and non-Pacific sea surface temperature solely through thermal exchange in (2.5), based on the amplitude of the atmospheric thermal (baroclinic) streamfunction. The surface temperature fields influence the atmospheric baroclinic mode in (2.1)–(2.2) through heat exchange. The atmosphere directly influences the North Pacific SST in (2.6) by thermal exchange and by Ekman-current advection. The atmosphere also indirectly influences North Pacific SST by its influence on geostrophic-current advection, since the atmosphere directly forces the top layer of the quasi-geostrophic Pacific Ocean flow in (2.12) via wind-stress curl variability. The top-layer streamfunction of the quasi-geostrophic ocean model advects the Pacific SST field in (2.6). The Pacific SST field only indirectly influences the underlying QG currents insofar that it alters the flow field of the overlying atmosphere. Since each model component is forced by a steady space-dependent forcing function, determined empirically from either observations or uncoupled simulations, the model climatologies are "close" to those which are observed (Roads 1987a, 1989b).

The atmospheric model variables in (2.1), (2.2) and (2.5) are spatially resolved with triangular-21 spherical harmonic representation. In physical space, the atmospheric variables ψ_1 and ψ_3 are then spectrally transformed to an approximately 5.5° Gaussian grid. Since the Pacific Ocean model variables in (2.6), (2.12) and (2.13) are resolved to 1°, whenever atmospheric variables are required to determine oceanic forcing functions, they are linearly interpolated from the 5.5° transform grid to the Pacific Ocean grid. This is more economical than transforming from spectral representation directly to a 1° grid. When Pacific Ocean SST is determined, the T_m values for Pacific grid points in (2.6) are first smoothed, by averaging with a hexagonal, 7 by 7 grid with each point weighted equally, and then substituted in the lower resolution atmospheric grid, which resolves (2.5).

The atmospheric model is integrated with a 1-hour time step. Once per day, the surface temperature field is computed and the Pacific Ocean subroutine is called. The QG currents and Pacific SST fields are then computed with a computationally stable, 12-hour time step. The land and non-Pacific surface-temperature field is computed using a 1-day time step, which causes a spurious 2-day, damped oscillation in land surface temperature because the response time for land temperature, $K_g^{-1} = 0.5$ days, is less than the time step. Analytical solution of the finite-difference equations for fixed T_a yields a land temperature response of the form $\exp[-(n\Delta t/K_g') + i(n\Delta t)]$, where the effective value of the land thermal exchange coefficient is $K_g' = \ln(1 - K_g\Delta t)/\Delta t \approx (3\text{ day})^{-1}$, for the 1-day time step. The spurious oscillation in the land T_m has an amplitude of the order of the instantaneous value of $(T_a - T_m)$. To explore the effect of this spurious oscillation, we recomputed Case A with land temperature properly resolved in time and found that it was climatologically indistinguishable from the case with the spurious oscillation. To show the character of the spurious oscillation, typical time series of air temperature (dashed) and land temperature (solid) at a location on North America are shown in Fig. 5 for these two runs. The character of the spurious oscillation is evident in the solid line of Fig. 5a and is similar to the aforementioned approximate analytical solution. Although the dashed lines in Figs. 5a and 5b differ in detail because they represent randomly selected time intervals from the two different runs, the character of the air temperature variability (dashed line) is similar for the two cases and further suggests that there is no serious difference between the air temperature variability over land between the two runs. Thus since the atmospheric response to this 2-day (biurnal) land temperature variability is both weak and well resolved, there is minimal impact (§4c) of this high frequency variability of land T_m on the predictability of the coupled system. Roads (1989b) also discussed its negligible influence on other low-frequency atmospheric events in Case A.

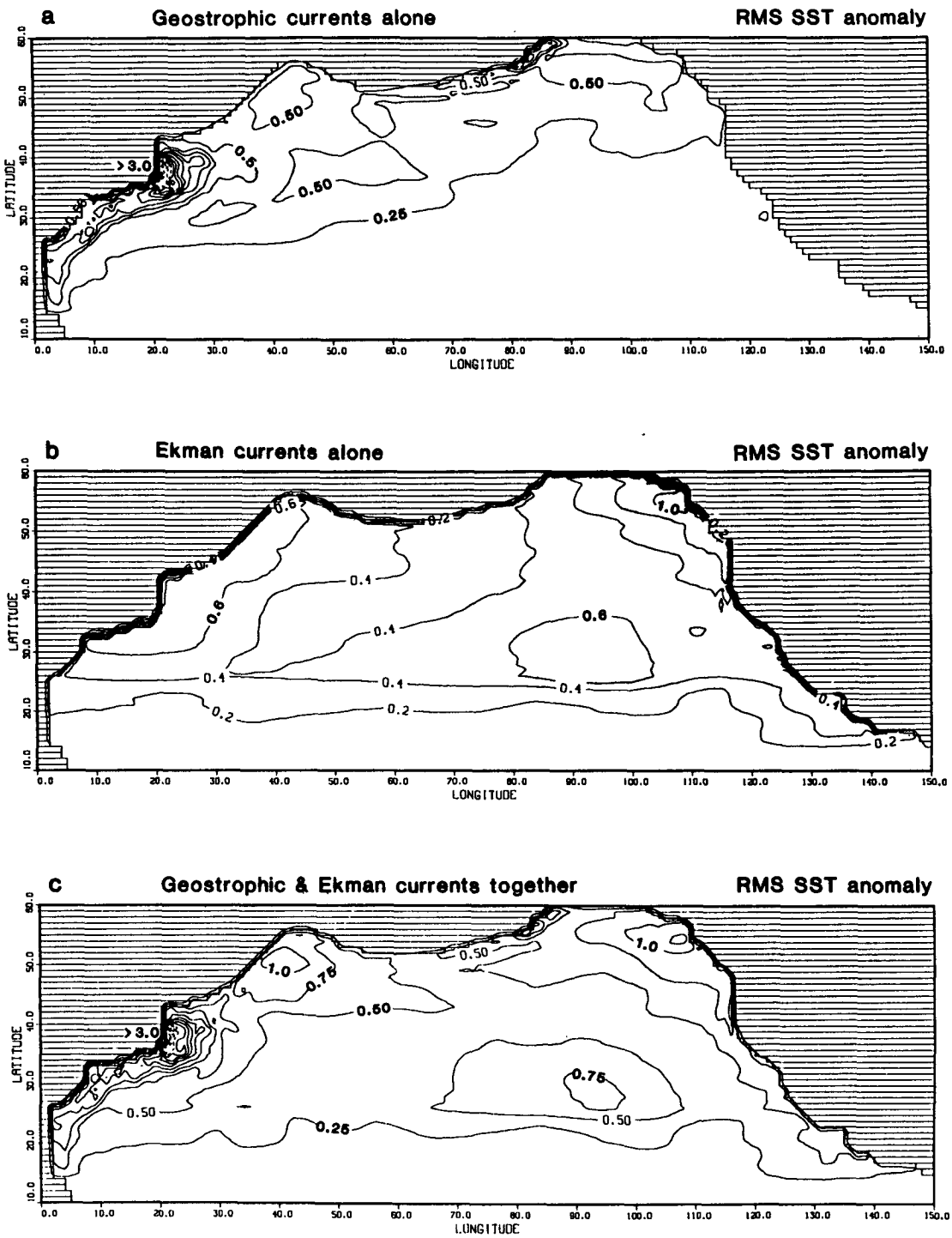

FIG. 3. Standard deviations of SST anomalies for five model years of uncoupled perpetual-January conditions generated by (a) geostrophic currents alone (CI = 0.25°C), (b) Ekman currents alone (CI = 0.2°C) and (c) geostrophic and Ekman currents together (CI = 0.25°C). In each case the anomalies are linearly damped with an effolding time scale of 58 days. The local maximum in (b) in the central eastern Pacific is due to the pulsating atmospheric vortex which occurs in the atmospheric model (cf. Fig. 2a). Monthly averaged SST anomaly rms fields look extremely similar to these fields, except for a slight amplitude reduction which is typically less than 10% of the values shown above.

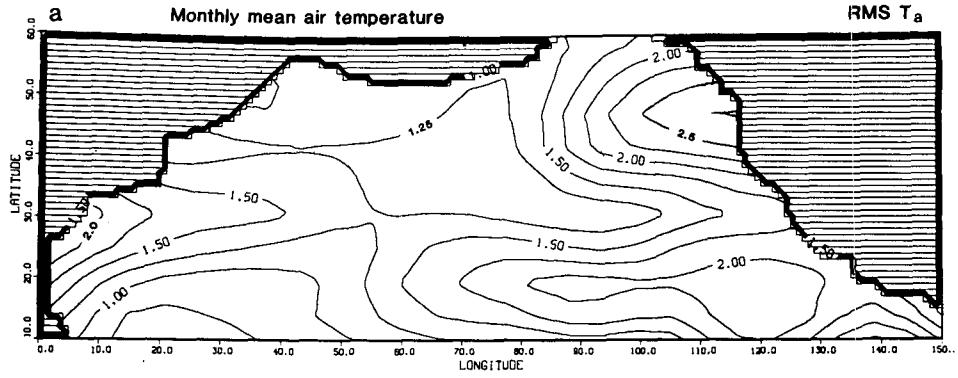
a
Monthly mean air temperature
RMS T_a
LATITUDE
LONGITUDE

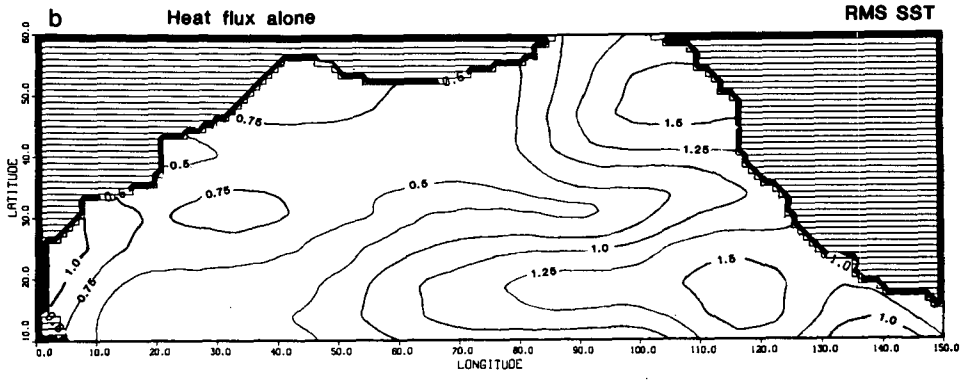
b
Heat flux alone
RMS SST
LATITUDE
LONGITUDE

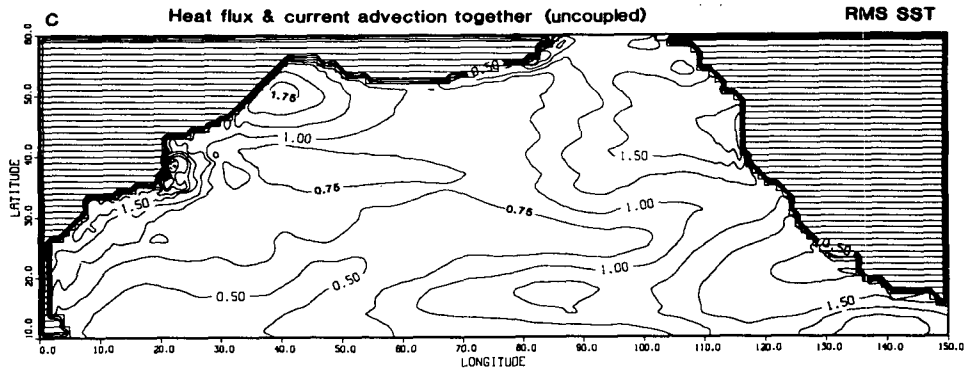
c
Heat flux & current advection together (uncoupled)
RMS SST
LATITUDE
LONGITUDE

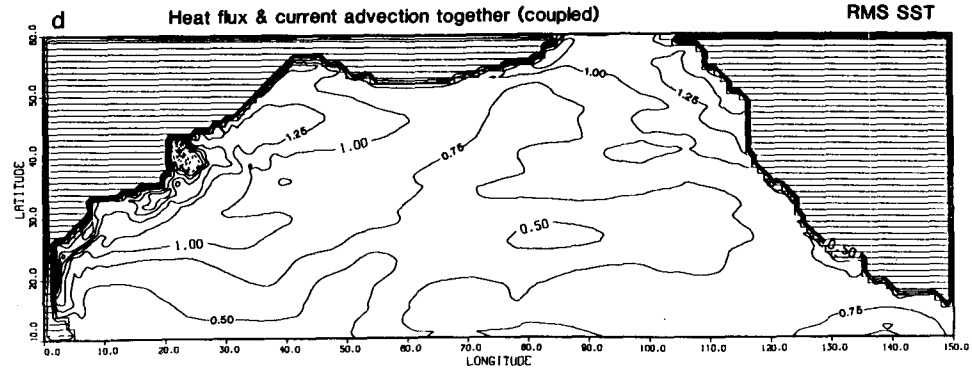
d
Heat flux & current advection together (coupled)
RMS SST
LATITUDE
LONGITUDE

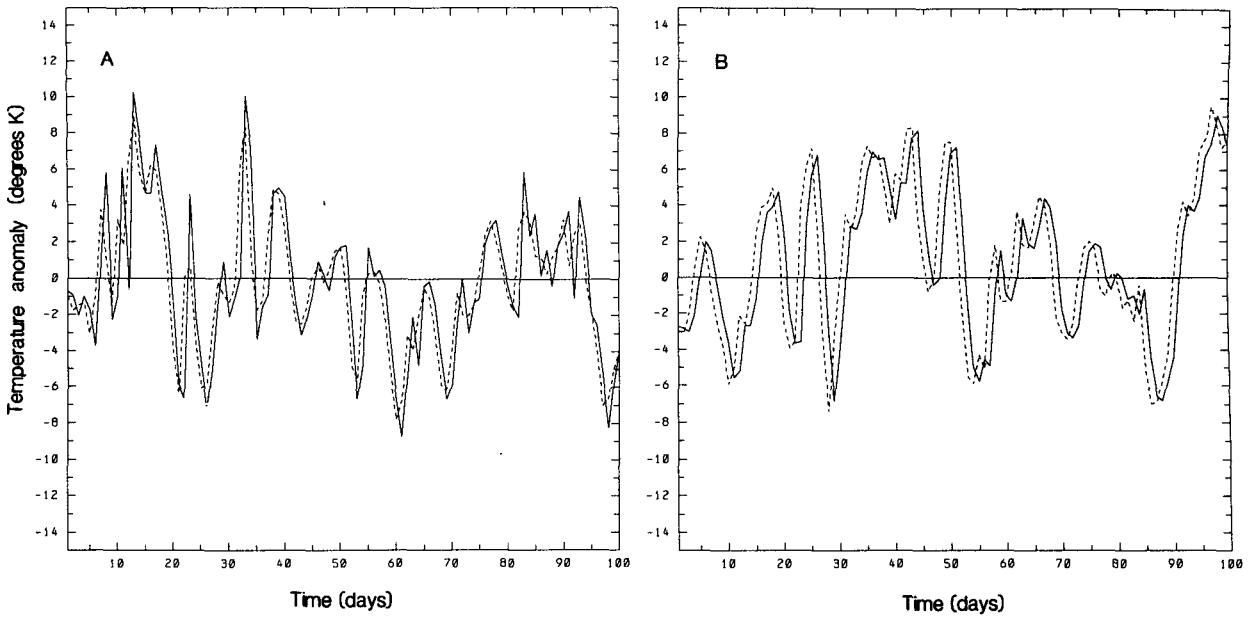

FIG. 5. Randomly selected intervals of the typical time variability of air temperature T_a (dashed lines) and land temperature T_m (land) (solid lines) at a grid point in New Mexico, for Case A executed (a) with and (b) without the spurious 2-day oscillation in T_m (land). The spurious oscillation is evident in the solid line of (a). Although the dashed lines in (a) and (b) differ in detail because they represent randomly selected time intervals from different runs in statistical equilibrium, the variations of the air temperature are similar for both runs. No significant differences in the mean or second-order statistics were detected between runs with and without the spurious oscillation. See text and Roads (1989b) for discussion.

3. Climatology

Five coupled systems were developed and examined during the course of this study (Table 1). In each coupled system herein discussed, Atlantic and Indian ocean SST variability is due solely to heat fluxes as determined by (2.5). First, we describe the spinup of the models and then the climatological characteristics. Since only three of the five systems are used in systematic extended-range predictability investigations, only brief comments concerning the remaining two systems are given.

The atmospheric model was initially spun up independently of the ocean (Roads 1987a) and energetic diagnostics indicated the system was in statistical equilibrium. In coupled mode, Case A was spun up 1 model year before a 5-year base run was executed and saved. That run served as the forcing function for test cases of the ocean model response. A similar spinup procedure was followed for Case E, although the base run was 6 years long. The QG ocean model was first integrated for 10 years with the mean forcing, then, along with the SST model, for an additional 5 years in uncoupled mode using the fluctuating forcing specified from Case A. The system of Case D was then integrated in coupled mode for 6 years to provide us with three 2-year intervals of simulated data for which we computed time mean fields and found little change between the second and third interval. A subsequent 6-year run, which formed Case D, found little difference among the 2-year means. A similar procedure was used for the 6-year runs of Cases B and C.

The first model we investigated (Case A) has been discussed by Roads (1989b). The heat transfer coefficient, K_g, for this case is shown in Fig. 1a. Heat fluxes alone are responsible for SST variability throughout the hemisphere. In the subsequent four models, the only changes are that the Pacific Ocean model (2.6) is invoked north of 10° latitude and the K_g field can differ.

The second model (Case B) replaces the "heat-flux only" Pacific SST model with an "advection only" SST model, wherein both Ekman and geostrophic currents contribute to the SST variability according to

FIG. 4. (a) Standard deviations of the monthly mean model atmospheric temperature field, T_a (CI = 0.25°C). Standard deviations (rms values) of monthly mean SST anomalies generated in uncoupled mode by (b) heat-flux variability alone and by (c) the combined effects of Ekman-current advection, geostrophic-current advection and heat-flux variability (CI = 0.25°C). (d) Same as (c) except in coupled mode (Case D) so that the atmosphere responds to the changing SST. Note the reduction in SST variability, particularly in the northeastern and northwestern basin, when running in coupled mode. Typical observed open-ocean values of January SST anomalies are 0.6 to 0.9°C (Cayan 1980).

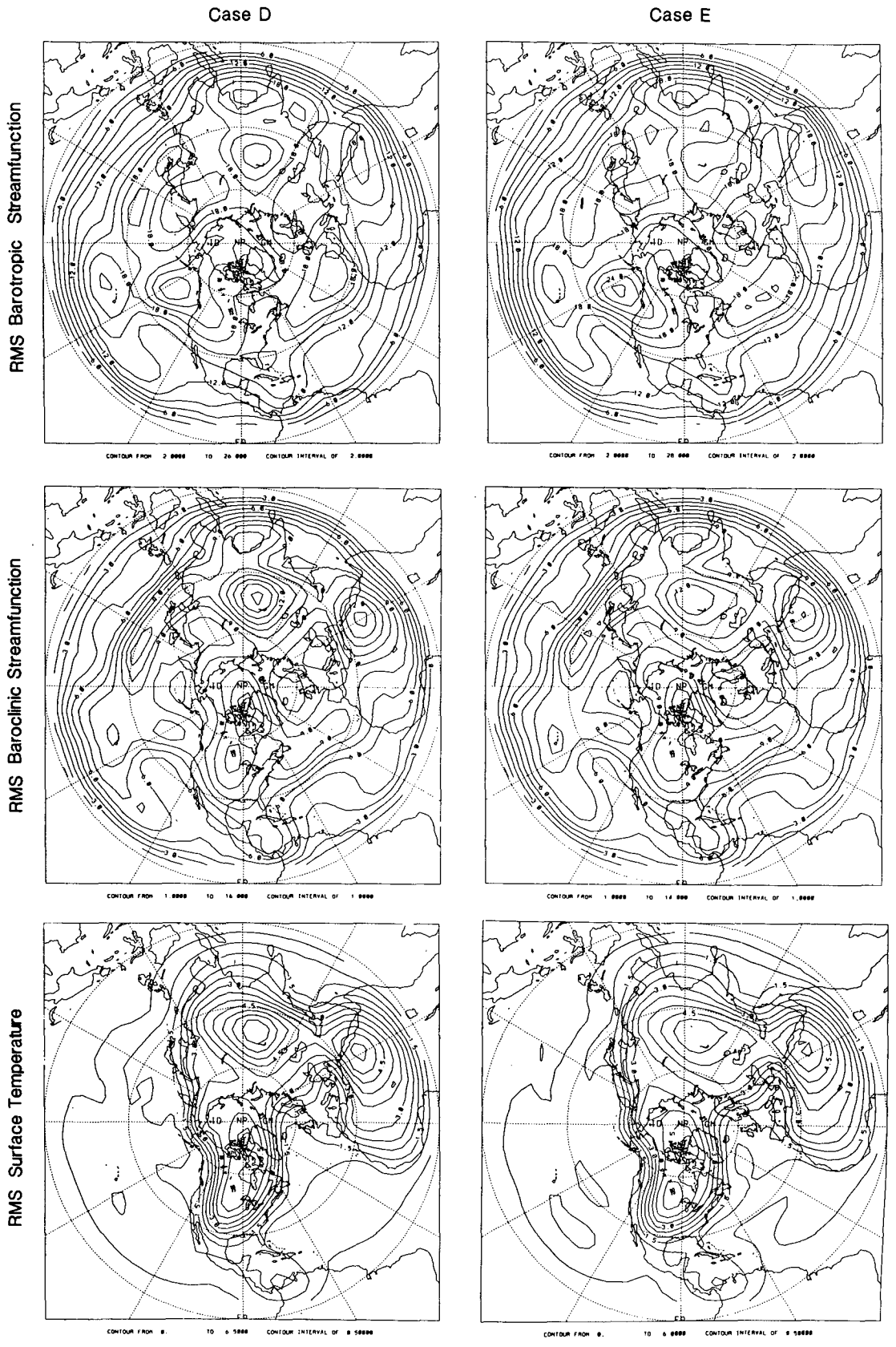
Case D
Case E
RMS Barotropic Streamfunction
RMS Baroclinic Streamfunction
RMS Surface Temperature

$$\frac{\partial T_m}{\partial t} + J(\phi_1, T_m) + A\nabla\psi_3 \cdot \nabla T_m = -K_g T_m + \kappa\nabla^2 T_m + F_{m_5} \quad (3.1)$$

where

$$F_{m_5} = A\nabla\bar{\psi}_3 \cdot \nabla\{T_m\} + J(\bar{\phi}_1, \{T_m\}) + K_g\{T_m\} - \kappa\nabla^2\{T_m\}. \quad (3.2)$$

Shifts in the time-averaged fields of atmospheric barotropic and baroclinic streamfunction were less than O(10%) of the amplitude of mean flow variables from Case A. This is the benefit of using steady state residual forcing functions for each component of the model which are designed to drive the system "close" to the observed flow patterns. Rms variability of the atmospheric variables generally decreased across the Pacific, North America and the North Atlantic. Neither the shifts in mean nor rms flows were significant at the 95% level of confidence, based on a simple F-test.

For Case A and B, the land/ocean boundary was demarcated by a linearly sloping interpolation between the K_g values over land and sea (Fig. 1a). This (at least to the oceanographer of this study) represented an intolerable reduction in the total areal influence of the ocean's slowly varying surface temperature. A new K_g was therefore constructed which allowed the spherical harmonic reconstruction of K_g at all Pacific Ocean points, as defined by the ocean model, to be very close to the open-ocean value of $(58\ \text{day})^{-1}$. This was accomplished by requiring that the land value of $K_g = (0.58\ \text{day})^{-1}$ only apply to points greater than 1000 km from ocean points. The linear slope of K_g from "ocean" to "land" values was then displaced a suitable distance from the ocean (Fig. 1b). This region can be regarded as a 1000 km-wide "marine layer," predicated by the low resolution ($\approx 5.5°$) of the atmospheric model.

Case C implemented the revised field of K_g shown in Fig. 1b, while again using the "advection-only" SST model in the Pacific. The variance of the atmospheric variables over the northeast Pacific was reduced relative to Cases A and B, particularly in the monthly averaged fields, but was still stronger than observed. The rms fields for this case again were not sufficiently different from the previous cases to be judged significant; a simple F-test typically requires a ratio of monthly averaged variances which exceeds 1.5, for the O(70) degrees of freedom involved, to have 95% confidence that the variance levels differ. Note that modeled atmospheric transients in the northeast Pacific region are often too energetic relative to observations both in more sophisticated GMCs (e.g., Schubert and Suarez 1989; Malone et al. 1984) as well as in the present model (Roads 1987a,b, 1989b).

The fourth case (D) forms the central basis for subsequent predictability studies and includes both heat-flux forcing and ocean-current advection in driving the Pacific SST variability, implements the new K_g field (Fig. 1b), and is run through the Pacific Ocean model 7 by 7 degree hexagonal filtering procedure (section 2.b). Cases D and E are then directly comparable to each other in the predictability results. Figures 6 and 7 show the total rms and monthly-averaged rms variability, respectively, for these two cases. The reader can examine differences and similarities between these two cases, Case A, and the observations by comparing Figs. 2 and 3 of Roads (1989b) with Figs. 6 and 7 here. The monthly averaged SST variability shown in Fig. 7 for Cases D and E has typical amplitude in the North Pacific which is less than that of Case A (Roads 1989b), and is more comparable to the observed values (0.6°–0.9°C) of Cayan (1980). This is because the new K_g field for these two cases causes the amplitude of rms SST near the countinental boundaries to decrease since the longer SST response time there filters out the higher-frequency variability of the heat-flux forcing, because the SST in Case E is just a low-pass filtered version of the baroclinic streamfunction variations. (Thus, there is a minimum of rms SST in Case E along 30°N northeast of Hawaii.) The ocean currents of Case D increase the open-ocean rms SST variability in the northern Pacific basin by about 50% of that in Case E. Differences in atmospheric rms variability among the five cases are not significantly different at the 95% level, except that the larger rms value of atmospheric baroclinic streamfunction that occurs over Asia for Case D is significantly larger than any other case.

4. Predictability experiments

a. Error-growth analyses

After integrating the coupled systems to statistical equilibrium (based on energetics and on the inspection of sequences of 2-year means), base runs, taken to represent observed fields, were integrated for 5 or 6 years (depending on the case) under perpetual-January conditions. At 30-day intervals, single predictability runs using the coupled model were initiated with error imposed in the atmospheric fields (wavenumbers greater than 11 set to climatic states), and with zero initial error in the ocean and land temperature models. The procedure was then repeated using the same initial conditions and atmospheric model but with the SST

FIG. 6. Root-mean-square, hemispheric distributions of (top to bottom) atmospheric barotropic streamfunction, ψ (scaled by 10^{-4}, CI = 2), atmospheric baroclinic streamfunction, τ (scaled by 10^{-4}, CI = 1), and surface temperature, T_m (CI = 1°C), for (left) Case D, which includes ocean-current and heat-flux variability in the Pacific SST equation and (right) Case E, which includes only heat fluxes in SST variability. Roads (1989b) shows the corresponding fields for Case A and for the observations.

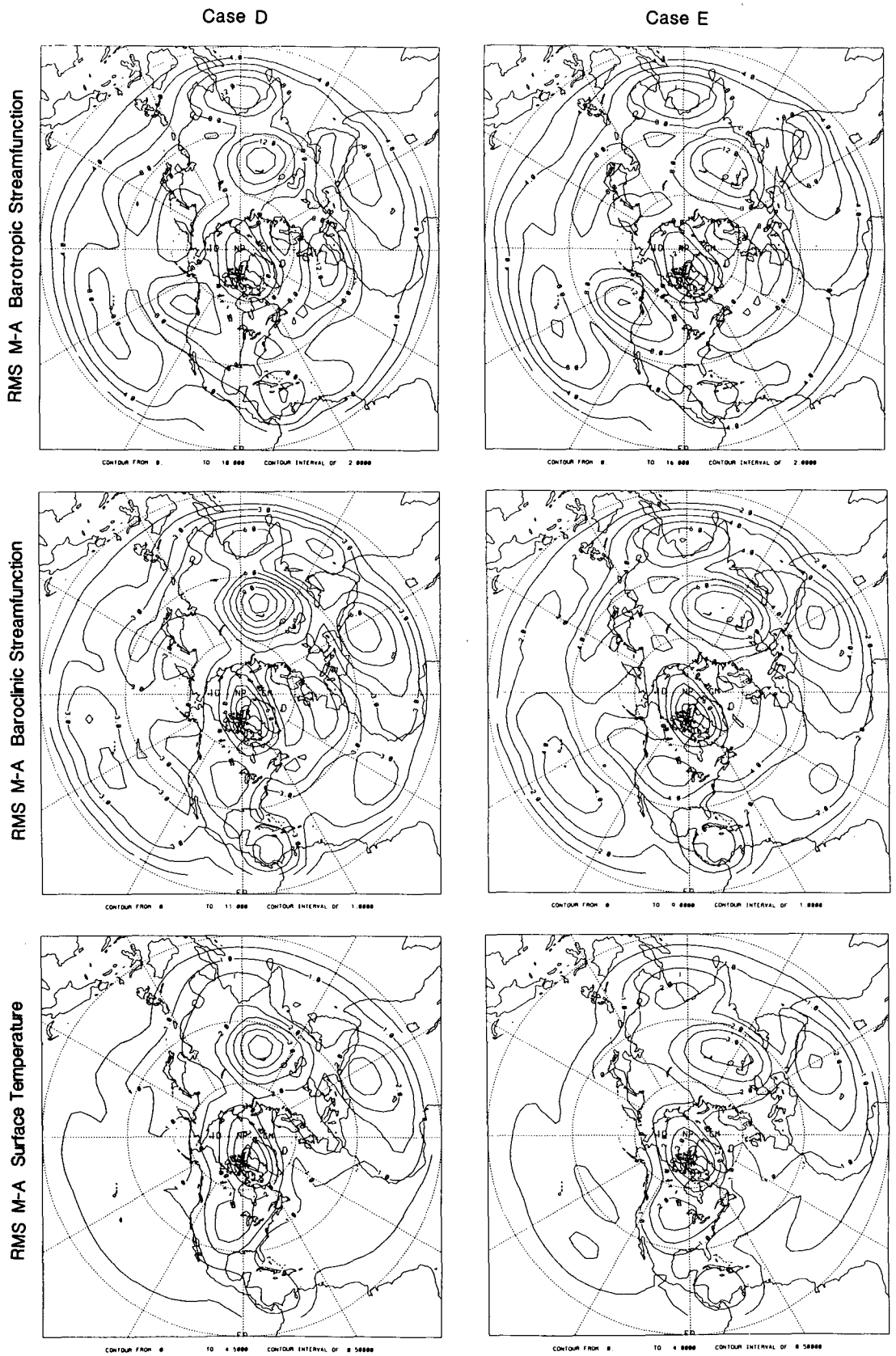

FIG. 7. Same as Fig. 6 but for monthly averaged quantities.

at ocean points (where $K_g \leq 2 \times 10^{-3}$) specified according to the other prediction models (section 1). In all cases, the land temperature (points where $K_g > 2 \times 10^{-3}$) was dynamically predicted after initialization.

Error-growth analyses included evaluating normalized anomaly correlation

$$\rho \equiv \frac{[\chi_o \chi_p] - [\chi_o][\chi_p]}{([\chi_o^2] - [\chi_o]^2)^{1/2}([\chi_p^2] - [\chi_p]^2)^{1/2}} \quad (4.1)$$

and root-mean-square error

$$E \equiv [(\chi_p - \chi_o)^2]^{1/2} \quad (4.2)$$

where χ_o and χ_p are "observed" and predicted space-dependent fields, respectively, and $[\cdot]$ indicates integration over the spatial domain of interest, generally either the hemisphere or the Pacific region (north of 10°). For instantaneous predictions, we computed ensemble averages of the correlation, $\langle \rho(t_d) \rangle$, and rms error, $\langle E(t_d) \rangle$, for each day t_d from 1 through 90 for typical sample sizes of 57 to 66. For time-averaged predictions, we computed the same statistics for averages from day 0 through day T, where $T = 1, \cdots, 90$.

In order to estimate the statistical significance of $\langle \rho(t_d) \rangle$, we use the Fisher Z transformation

$$Z \equiv \frac{1}{2} \ln \frac{(1 + \rho)}{(1 - \rho)} \quad (4.3)$$

which, in general, has a distribution around the ensemble mean which is more Gaussian than that of (4.1). We tested the distributions of time-averaged Z for non-Gaussianity and these tests indeed failed. We can therefore assume that Z is normally distributed so that 68% confidence intervals on the estimation of $\langle Z \rangle$ are

$$\pm \Delta Z = \pm \left(\frac{\mu}{(N/T_o)} \right)^{1/2} \quad (4.4)$$

where μ is the variance of Z around $\langle Z \rangle$, N is the number of members of the ensemble and T_o provides a measure of independence of ensemble members. Following Leith (1973), $T_o = 2/\nu$ where $\nu = -\ln \langle Z(1)Z(0) \rangle / \langle Z(0)^2 \rangle$, $Z(1)$ is a given forecast of Z and $Z(0)$ is the previous forecast. Additionally, it is required that $1 \leq T_o \leq N$ (see also Roads 1989a). Only for predictions of time-averaged SST that approach 3 months, did T_o significantly exceed unity.

If $\langle Z \rangle$ exceeds ΔZ we claim that $\langle Z \rangle$ is nonzero with 68% confidence. If we estimate $\langle Z \rangle$ from two different prediction models and assume that μ is identical for both cases, the difference between the two ensemble means must exceed $\sqrt{2}\Delta Z$ for us to cliam that the difference is nonzero with 68% confidence. For such comparisons, we use the maximum μ of the two cases for computing ΔZ. We henceforth define an estimate to be "marginally significant" (68% confidence) when the $\langle Z \rangle$ estimates differ by approximately $\sqrt{2}\Delta Z$. Similarly, we define a "significant" difference (95% confidence) to be when estimates differ by approximately $2\sqrt{2}\Delta Z$. The baseline of no skill for a prediction model is defined to be when the $\langle Z \rangle$ of the given prediction model is not significantly different from the $\langle Z \rangle$ associated with atmospheric persistence of day zero.

b. *Predictability of instantaneous fields*

Instantaneous predictability is defined to be the ensemble-averaged skill value, measured by (4.1), (4.2) or (4.3), for predictions made for a given field's instantaneous values on a given day. Roads (1987a) has discussed the general properties of $\langle \rho \rangle$ for the case of the uncoupled atmosphere and found that the character of model error-growth times was comparable to the observed atmosphere. The main difference between the error-growth characteristics of this atmospheric model and present-day numerical weather prediction models is that the initial error is generally smaller in the present model.

Results from each of the three cases (A, D, E) for which we explored instantaneous predictability are consistent with no significant enhancement to the predictability of the coupled model atmosphere, compared to the uncoupled atmosphere of Roads (1987a). We concentrate our discussion on Case D, which is the most realistic and which generally has the largest improvements in predictions, presumably due to the larger rms SST variability in the Pacific.

Figure 8 shows the typical correlation decay with time for the atmospheric streamfunctions for coupled model predictions and predictions based on persistence of the atmosphere from day zero. The corresponding plots for Pacific SST are shown in Fig. 9. After approximately day 18, dynamical predictions of atmospheric streamfunction for the hemisphere, based on any of the practical prediction models (i.e., climatic SST model, persistent SST model, coupled model), differ insignificantly (68% confidence) from predictions based on atmospheric persistence. However, if anomalous SST is specified (true SST) and the resulting dynamical predictions are compared to those wherein SST is specified to be the climatological values (climatic SST), there is a marginally significant improvement in $\langle Z \rangle$ after day 15 (Fig. 10) through day 18 when atmospheric persistence is no worse than the dynamical prediction. This suggests that it requires approximately 2 weeks for the atmosphere to recognize that it is flowing over an anomalous midlatitude SST field.

Instantaneous predictability of the Pacific SST field using the coupled model represents only a weak improvement over predictions based on SST persistence (Figure 9). After approximately day 15, means of these two predictions for case D only differ with marginal significance (68% confidence) and by day 45 the two curves cross. SST is actually more persistent in the Pa-

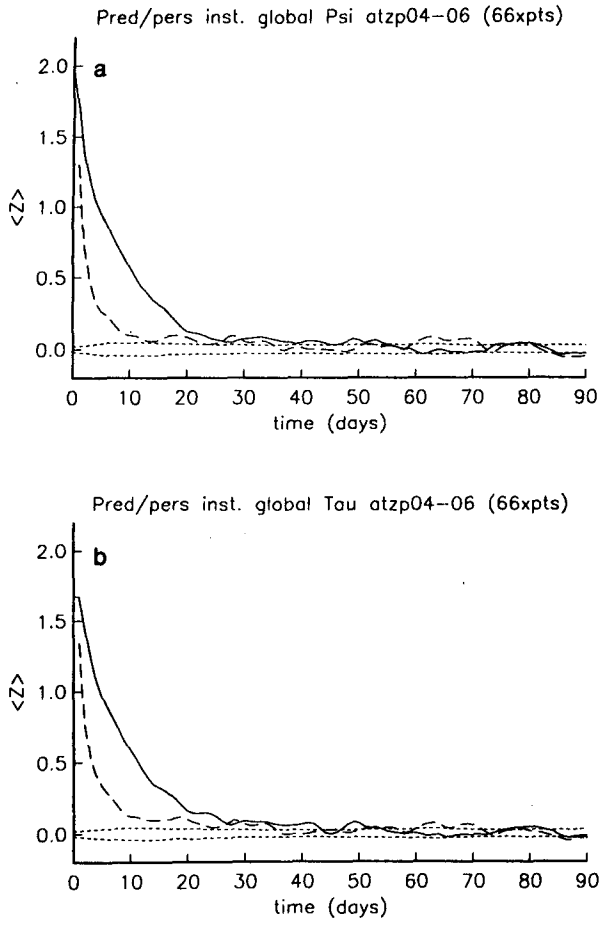

FIG. 8. Ensemble-averaged Fisher z values, $\langle Z \rangle$, defined by (4.3), as a function of prediction day for instantaneous fields of (top) atmospheric barotropic and (bottom) atmospheric baroclinic streamfunction for the hemisphere for Case D, which includes ocean currents in the Pacific SST equation. Solid line is the dynamical prediction using the coupled model, long dashed line is the prediction based on atmospheric persistence from day zero and the distance between the two short dashed lines equals $2\Delta Z$, defined by (4.4). After approximately day 18, the ensemble average of predictions based on the coupled model is not significantly different from that based on atmospheric persistence of day zero. Dynamical predictions which implement the "climatic SST" model and the "persistent SST" are slightly, but not significantly, lower for days 10 through 25.

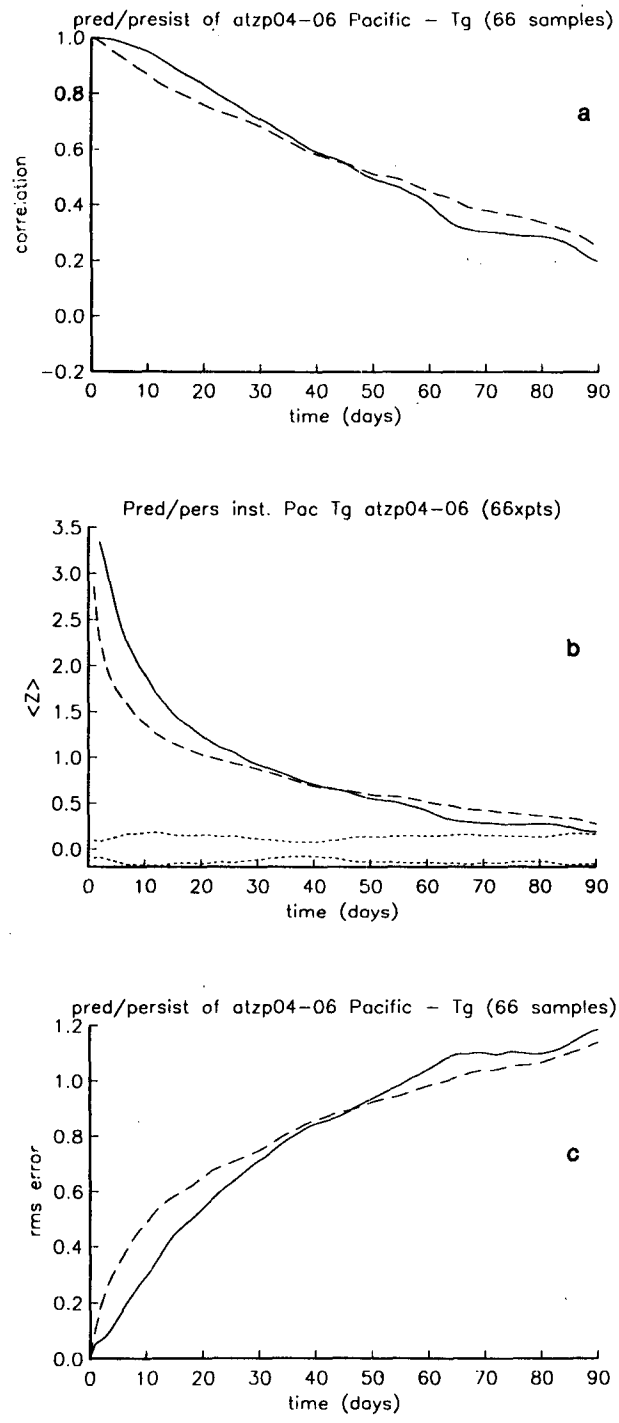

FIG. 9. (a) Ensemble-averaged correlation $\langle \rho \rangle$, defined by (4.1), as a function of prediction day for instantaneous fields of Pacific Ocean SST field for Case D, which includes ocean-current and heat-flux variability in the Pacific SST equation. Solid line is dynamical prediction based on the coupled model, while the long-dashed line is based on SST persistence of day zero. (b) Same as (a) but for $\langle Z \rangle$, showing the effect of the transformation (4.3). (c) Same as (a) but for rms error. The distance between the two short dashed lines equals $2\Delta Z$, defined by (4.4). After approximately day 15, the dynamical prediction of SST is not significantly different from the prediction based on SST persistence of day zero.

cific than for the hemispheric oceans, apparently due to heat-flux forcing by a slowly varying atmospheric baroclinic wave in the eastern Pacific (Roads 1989b). Clearly, since the model ocean is purely atmospherically forced, and since the predicted atmospheric flow fields rapidly become erroneous, dynamical predictions of SST using a coupled model cannot much improve upon the strongly persistent nature of the SST field.

c. *Predictability of time-averaged fields*

In contrast to predictions of instantaneous fields, we find many significant results for the time-averaged

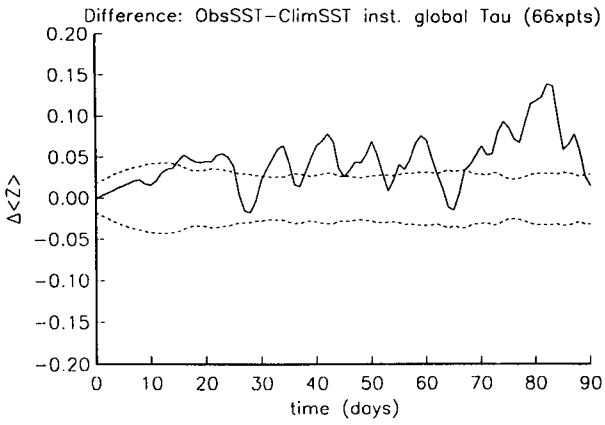

FIG. 10. Solid line is the difference between $\langle Z \rangle$ for predictions based on the "true SST" prediction model and climatic SST prediction model for instantaneous hemispheric baroclinic streamfunction for Case D. The distance between the two short dashed lines equals $2\Delta Z$, defined by (4.4). By day 15, there is a marginally significant difference between the two models. By considering Fig. 8, it is evident that after day 18 or so, ΔZ loses meaning, since dynamical predictions are not significantly different from predictions based on atmospheric persistence of day zero.

fields. Again, we concentrate our discussion on Case D, which is the most realistic and which generally exhibits the largest improvements in predictions, apparently due to the larger rms SST variability in the Pacific. Results are generally less significant for Case E and least significant for Case A, which suggests that time-averaged atmospheric predictability depends in part on the magnitude, areal extent and/or generating mechanism of SST variability, although we have not explored these dependencies.

Figures 11a,b shows typical plots of the correlation decay versus time-averaging interval for coupled model predictions of time-averaged, hemispheric, atmospheric streamfunctions. For time averages longer than approximately 60 days, the mean values of $\langle Z \rangle$ are not significantly different from those based on atmospheric persistence from day zero. Predictions for atmospheric flow fields over the Pacific are significantly less persistent and less predictable than the hemispheric fields, possibly because the model atmosphere has more variability in the stormtrack. It is interesting to compare the intrinsic predictability of the coupled model with estimates of predictability from more complicated GCMs. For example, 30-day average predictions of January 500 mb height have been examined in theoretical predictions of the NCAR CCM0B by Tribbia and Baumhefner (1988) and in hindcast experiments with the Canadian Climate Centre model by Boer (1989). For the analogous field of 30-day averaged barotropic streamfunction in the Northern Hemisphere we found the 66-member ensemble mean of the anomaly correlation coefficient to be 0.52 for the coupled model. Tribbia and Baumhefner (1988) found a value of 0.47 for a 20-member ensemble while Boer (1989), after removing system error, found an ensemble averaged hindcast skill of approximately 0.5 for lagged-averaged predictions of eight Januaries.

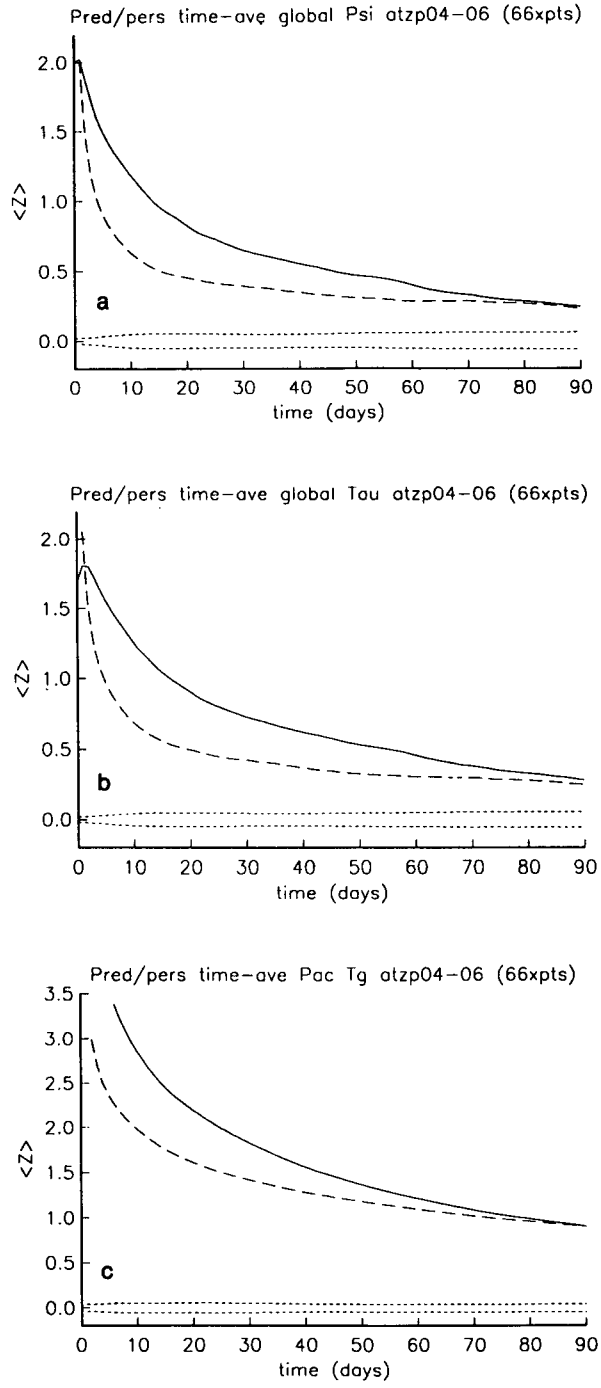

FIG. 11. (a,b) Same as Fig. 8 but for time-averaged atmospheric streamfunction and (c) for time-averaged Pacific Ocean SST. The ordinate represents time-averaging interval, averaged from day zero to day T, with $T = 1, \cdots, 90$. Coupled model predictions of time averages longer than approximately 60 days are not significantly different from predictions based on atmospheric persistence of day zero.

The dynamical predictions of time-averaged Pacific SST are significantly better than predictions based on SST persistence only for averages of 60 days and less, while hemispheric SST is at least marginally significantly better than SST persistence for up to 90-day averages. Namias et al. (1988) discuss the persistent nature of observed North Pacific SST and find that the correlation between monthly mean January SST anomalies and the subsequent monthly mean is 0.62. The correlation between the 30-day averages of model SST anomaly and persistence predictions (Fig. 11c) is greater (0.87) than the Namias et al. estimates mainly because it represents persistence of day zero, rather than persistence of the previous monthly mean. The SST observations, however, are influenced by various small-scale processes which are neglected in this model. In addition, the observations must contain some error and thus may underestimate the performance of SST persistence.

The performance of the coupled model for Case D is significantly better than the "climatic SST" model (Fig. 12) for predictions of 30- to 60-day averages of hemispheric and Pacific atmospheric fields. This result shows that shorter time averages fail to recognize the presence of the SST anomaly. Longer averages do not significantly differ from predictions based on atmospheric persistence of day zero.

The primary result from this analysis (Fig. 13) is that the improvement in predictions of atmospheric variables using the coupled model is not significant compared to atmospheric predictions using the "persistent SST" model. This result is a consequence of the atmospherically forced nature of the SST field, the dynamical predictions of which are only slightly better than SST persistence.

We also find that the atmospheric model forced by "true" SST fields is significantly better at predicting 2-month and longer averages than either the coupled prediction model or the persistent SST prediction model (Fig. 14). This result is most significant for Case D wherein the total variance of Pacific SST is 1.5 to 2 times larger than for the heat-flux only cases. Predic-

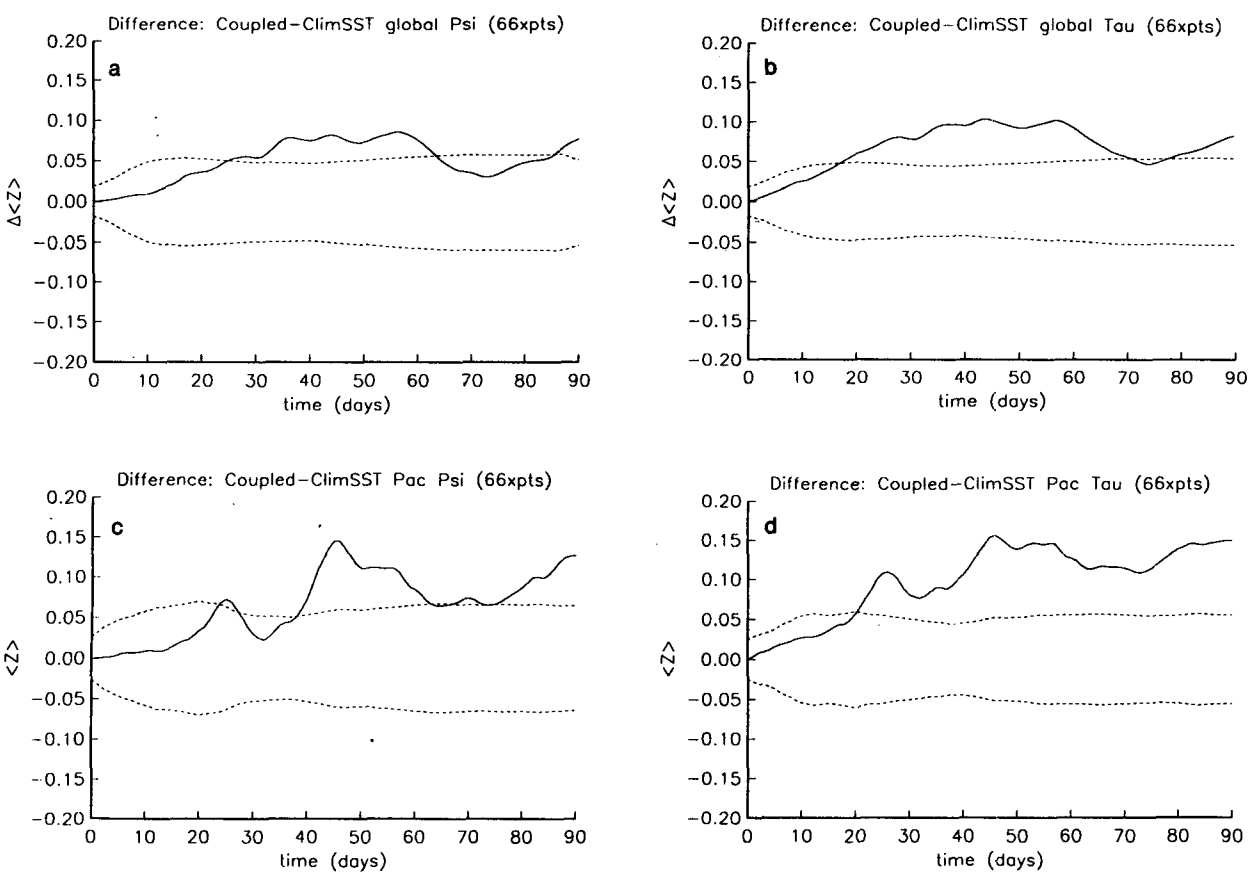

FIG. 12. Solid lines are the differences between $\langle Z \rangle$ for time-averaged predictions based on the coupled model and the climatic SST prediction model for (a) hemispheric barotropic streamfunction (b) hemispheric baroclinic streamfunction (c) Pacific barotropic streamfunction and (d) Pacific baroclinic streamfunction for Case D. The distance between the two short dashed lines equals $2\Delta Z$, defined by (4.4). The coupled model predictions are at least marginally significantly better than the climatic SST predictions for time averages between 30 and 60 days. Longer than 60-day averages predictions do not have significantly different skill than predictions based on atmospheric persistence of day zero (cf. Fig. 11).

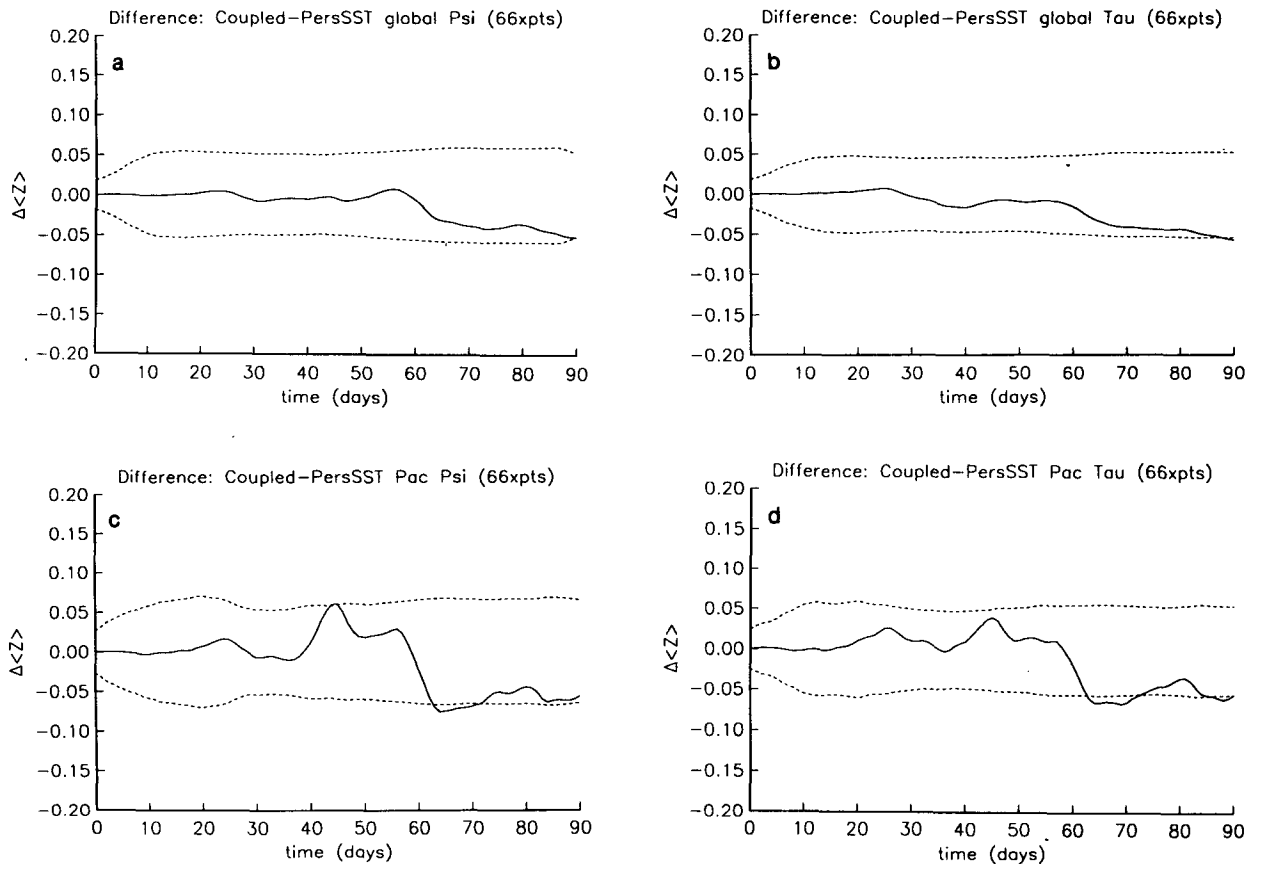

FIG. 13. Same as Fig. 12 but for difference between the coupled model and the "persistent SST" prediction model. The two prediction models perform with very similar skill. Longer than 60-day average predictions are not significantly different in skill from predictions based on atmospheric persistence of day zero (cf. Fig. 11).

tions of the atmospheric baroclinic streamfunction, which is forced directly by the SST field, are generally better predicted than the barotropic streamfunction. Furthermore, the improvement in predictions of fields over the Pacific are generally better than their hemispheric counterparts, although the Pacific fields are actually less predictable than the hemispheric fields.

Notice in Fig. 15 that the predictions from the true SST model are (at least marginally) significantly better than atmospheric persistence of day zero for all time averages through 90 days. Predictions of the North Pacific atmospheric barotropic and baroclinic streamfunction from the true SST model, account for roughly 12% and 25%, respectively, of the anomaly variance (i.e., square of the anomaly correlation) for 1-month through 3-month averaged fields. It is interesting to compare our results with those of Baumhefner et al. (1988), who showed ensemble averages of 30-day averaged 500 mb height anomalies hindcasted by the NCAR CCM1 for both observed SST and climatological SST during several winters. The analogous results found here are for barotropic streamfunction predicted using the true SST model vis-a-vis the climatic SST model. Their results, ensemble-averaged over 80 forecasts from eight different initial conditions, indicated average improvement of the anomaly correlation of about 0.04 for the Northern Hemisphere north of 20°N and about 0.10 for North America compared with improvements of about 0.06 found here for both the North Pacific and The Northern Hemisphere regions.

We also examined the linearity of the model ocean's response by computing the predictability of Pacific SST by specifying perfect atmospheric forcing functions with initial error included in the SST and ocean geostrophic current fields. The ocean's SST response, over time scales of a few weeks, gradually returned to nearly perfect correlation with the base run. This verified the dependence of the model ocean's response on the atmospheric forcing.

As mentioned in section 3, we inadvertently included a spurious two-day oscillation in land-surface temperature. We explored the predictability of Case A with and without the spurious two-day land-temperature oscillation. Both coupled systems were found to exhibit nearly identical intrinsic predictability for the atmospheric and oceanic variables. When SST was set to

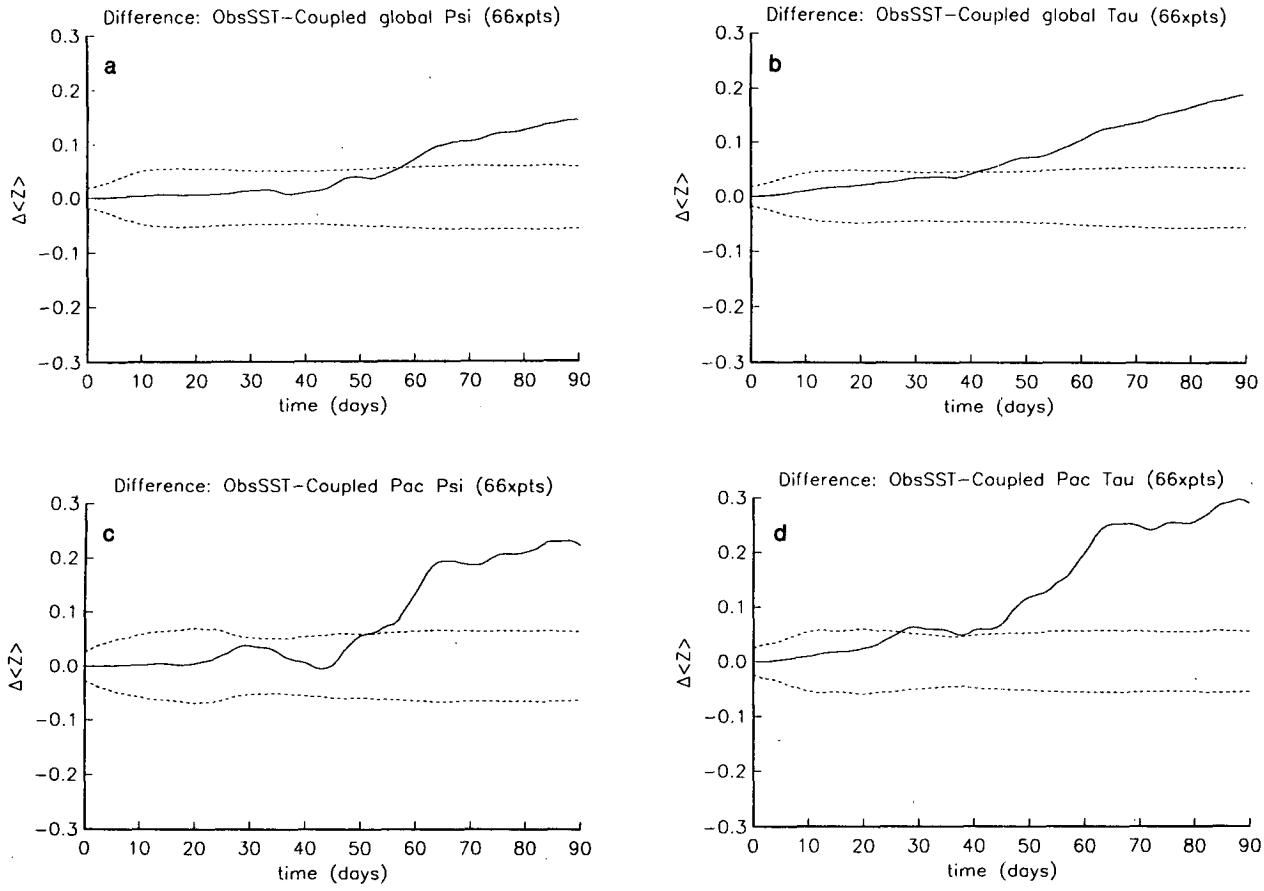

FIG. 14. Same as Fig. 12 but for difference between the true SST prediction model and the coupled model. For 60-day averages and longer, predictions of atmospheric variables based on the true SST model are significantly better than predictions using the coupled model.

the climatological values, however, and the resulting pair of coupled systems compared, the case with the spurious two-day land-temperature variability was found to be slightly less predictable than the case with well-resolved land temperature. This is because the unresolved land temperature represents a source of spurious high-frequency variability which causes land temperature to be somewhat less predictable than in the resolved case. Since both land and sea temperature contribute to the boundary forcing of the overlying atmosphere, turning off the SST variability in the unresolved case has a greater impact on predictions of the atmospheric circulation. Thus when SST is set to its climatological values, the predictability of the coupled system with the spurious two-day land-temperature variability is diminished relative to the resolved case because land temperature fails to force as strongly a slowly varying component of atmospheric flow. The cases discussed herein therefore represent viable estimators of the intrinsic predictability of coupled atmosphere–ocean systems although they include a component of high-frequency noise in land-temperature variability. The consequences on intrinsic predictability of other mechanisms for high-frequency variability, such as a diurnal cycle, are unknown.

5. Summary and discussion

We have examined the predictability of a simplified coupled model of large-scale atmosphere–ocean interaction, estimating statistical significance from large ensembles of experiments. The results suggest that there is no significant difference among the ensemble mean skill scores for predictions of *instantaneous* model fields using the four atmospheric prediction models (climatic SST, persistent SST, predicted SST and true SST) that we considered. We find, however, that the success of predictions of *time-averaged* model fields often depends significantly on the prediction model. Our results are summarized as follows:

1) SST anomalies influence the overlying atmospheric flow fields, with 68% confidence, after approximately 2 weeks in instantaneous atmospheric predictions and 3–4 weeks in time-averaged atmospheric predictions.

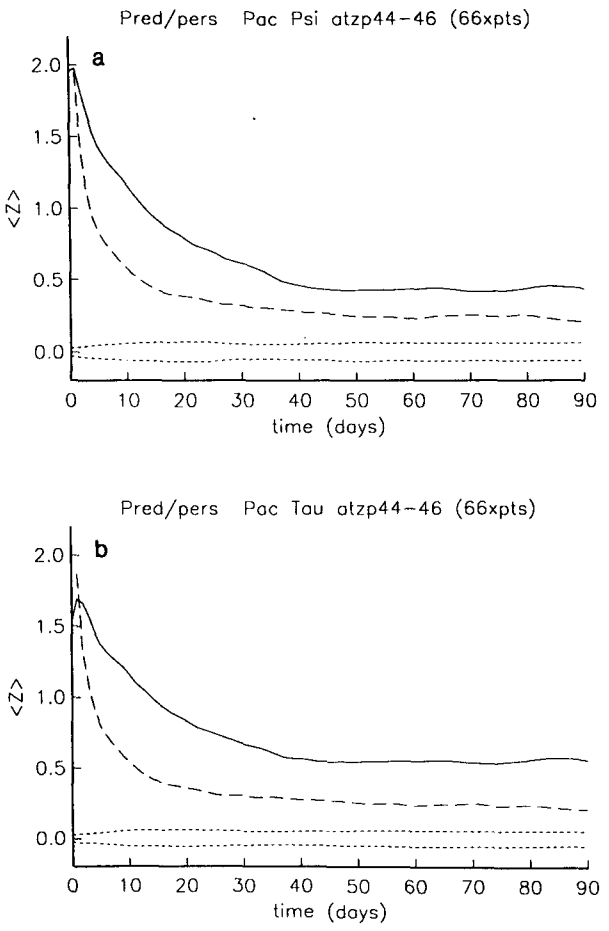

FIG. 15. Same as Fig. 11 but for the true SST prediction model of time-averaged atmospheric flow. For all the averaging intervals, the predictions based on the true SST model are significantly different from predictions based on atmospheric persistence of day zero.

2) If SST is specified from observations for hindcasting purposes we find that forecast skill is increased (at least marginally) significantly relative to predictions using climatic SST for both instantaneous and time-averaged atmospheric flow fields. The improvement in the skill relative to the climatic SST predictions increases steadily from 1-day to 90-day time averages. Roughly 20%–30% of the anomaly variance of 1-month through 3-month time averages of baroclinic Pacific flow fields, and somewhat lower percentages for hemispheric flow fields, can be expected to be dynamically predicted given the observed SST and an excellent atmospheric forecasting model.

3) Coupled atmosphere–ocean models have little chance of outperforming an atmospheric model with midlatitude SST specified by persistence of day zero. This applies to forecasting either instantaneous or time-averaged atmospheric fields for local or hemispheric regions. This result is because the atmosphere loses predictive skill on a time scale (3 days) which is comparable to that on which it responds to the thermal forcing of the ocean (5.3 days).

4) Dynamical predictions of midlatitude SST are expected to be only slightly better than predictions using SST persistence. This result is because the ocean is only forced by the atmosphere which, after about 2 weeks, provides erroneous forcing functions for the ocean flows (cf. the stochastic forcing models of Frankignoul and Hasselmann 1987).

Although the improvements in dynamical prediction are claimed to be significant, they are rather small. For time-averaged predictions using the coupled model vis-a-vis the climatic SST model, the enhancement to the anomaly correlation for time averages between 30 and 60 days is roughly 0.10 for Pacific fields, and half that for hemispheric fields. Longer-term averages do not differ significantly from atmospheric persistence of day zero. The atmospheric thermal field over the Pacific in Case D tends to exhibit the most marked improvements (coupled versus climatic SST), apparently because of the rather strong SST variability there. For 30-day and 60-day time averages of that field, the fraction of predicted anomaly variance increases, respectively, from roughly 25% and 5% for the climatic SST model, to 30% and 15% for either the coupled or persistent SST models. These predictions would be further enhanced by invoking model persistence at the point where the correlation of the dynamical prediction begins to drop more rapidly than persistence of day zero (Roads 1986). If we use the true SST model, which is impractical for forecasting, the predicted variance of 60-day averages increases to roughly 20% and longer-term time averages are as skillful as the 60-day averages.

We have excluded several effects which may alter our conclusions:

1) The heat exchange between the ocean and atmosphere may be strongly influenced by more realistic atmospheric boundary-layer and condensation parameterizations, causing the atmosphere to become more sensitive to the midlatitude SST anomalies.

2) The seasonal cycle of SST response may be very important in forcing the overlying atmosphere (Namias 1976) and, consequently, may influence time-averaged predictions (e.g., compare the 1976 to the 1978 statistical results of Davis).

3) The turbulent entrainment of thermal anomalies beneath the mixed layer can couple the slow evolution of oceanic baroclinic waves (upper-ocean heat content) to the mixed-layer variability, thereby imposing longer natural time scales on SST variability. However, the (unpredictable) atmospheric variables will, nonetheless, probably dominate that process.

4) The inclusion of ocean topography and non-linearity can support energetic, surface-trapped, geostrophic currents in the 50–100 day period band. In our model, this band is dominated by (unpredictable) Ekman currents. In the real ocean, advection by sur-

face-trapped geostrophic currents may be more predictable than was found here, because unstable ocean currents may have intrinsic predictability time scales which are longer than 2 weeks (e.g., Carton 1987; Malonotte-Rizzoli and Holland 1988).

5) Equatorial SST anomalies may significantly influence the predictability of the midlatitude atmospheric circulation through teleconnections (e.g., Mansfeld 1986; Owen and Palmer 1987; Shukla and Fennessy, 1988).

We will investigate these effects with more sophisticated models.

Acknowledgments. AJM was supported by an Andrew W. Mellon Foundation postdoctoral fellowship through the Climate Research Group and California Space Institute at Scripps. Additional support was provided by California Space Institute Grant 47-87, the Climate Analysis Center, NSF Grant ATM85-20540 and NOAA Grant NA86-AA-D-CP104. Supercomputing resources at the San Diego Supercomputer Center were provided by a grant from SDSC, the SIO Block Grant and the aforementioned NSF grant. We thank Bill Holland, Julianna Chow, Dan Rudnick, Dan Cayan, Bob Livezy and Dave Baumhefner for important input and discussion. We thank Shyh Chen, Phil Bogden, Dan Cayan and Mark Swenson for comments on the manuscript.

REFERENCES

Baumhefner, D. P., J. J. Tribbia and M. L. Blackmon, 1988: The influence of specified sea surface temperature and initial condition uncertainty on monte carlo extended-range forecast ensembles. *Modelling the Sensitivity and Variations of the Ocean-Atmosphere System,* Report of a Workshop at the European Centre for Medium-Range Weather Forecasts, WCRP-15, WMO/TD-No. 254, pp. 3–10.

Boer, G. J., 1989: A dynamical extended-range forecasting experiment with the CCC GCM. *Proc. 13th Annual Climate Diagnostics Workshop.,* U.S. Dept. of Commerce, NOAA, 398–402.

Carton, J. A., 1987: How predictable are the geostrophic currents in the recirculation zone of the North Atlantic? *J. Phys. Oceanogr.,* **17,** 751–762.

Cayan, D. R., 1980: Large-scale relationships between sea surface temperature and surface air temperature. *Mon. Wea. Rev.,* **108,** 1293–1301.

Davis, R. E., 1976: Predictability of sea surface temperature and sea level pressure anomalies over the North Pacific Ocean. *J. Phys. Oceanogr.,* **6,** 249–266.

——, 1978: Predictability of sea level pressure anomalies over the North Pacific Ocean. *J. Phys. Oceanogr.,* **8,** 233–246.

Frankignoul, C., and K. Hasselmann, 1977: Stochastic climate models: Part 2. Application to sea-surface temperature anomalies and thermocline variability. *Tellus,* **29,** 289–305.

——, and R. W. Reynolds, 1983: Testing a dynamical model for mid-latitude sea surface temperature anomalies. *J. Phys. Oceanogr.,* **13,** 1131–1145.

Horel, J., and J. O. Roads, 1988: Sensitivity of regional predictability to flow characteristics. *J. Geophys. Res.,* **93,** 11 005–11 014.

Leith, C. E., 1973: The standard error of time-average estimates of climatic means. *J. Appl. Meteor.,* **12,** 1066–1069.

Levitus, S., 1982: Climatological Atlas of the World Ocean, NOAA Professional Paper 13, U.S. Government Printing Office, Washington, D.C., 173 pp.

Malone, R. C., E. J. Pitcher, M. L. Blackmon, K. Puri and W. Bourke, 1984: The simulation of stationary and transient geopotential-height eddies in January and July with a spectral general circulation model. *J. Atmos. Sci.,* **41,** 1394–1419.

Malanotte-Rizzoli, P., and W. R. Holland, 1988: Data constraints applied to models of the ocean general circulation. Part II. The transient, eddy-resolving case. *J. Phys. Oceanogr.,* **18,** 1093–1107.

Mansfield, 1986: The skill of dynamical long-range forecasts, including the effect of sea surface temperature anomalies. *Quart. J. R. Meteor. Soc.,* **112,** 1145–1176.

Namias, J., 1976: Negative ocean-air feedback systems over the North Pacific in the transition from warm to cold seasons. *J. Phys. Oceanogr.,* **6,** 1107–1121.

——, X. Yuan and D. C. Cayan, 1988: Persistence of North Pacific sea surface temperature and atmospheric flow patterns. *J. Climate,* **1,** 682–703.

Owen, J. A., and T. N. Palmer, 1987: The impact of El Niño on an ensemble of extended-range forecasts. *Mon. Wea. Rev.,* **115,** 2103–2117.

Palmer, T. N., and S. Zhaobo, 1985: A modelling and observational study of the relationship between sea surface temperature in the northwest Atlantic and the atmospheric general circulation. *Quart. J. R. Meteor. Soc.,* **111,** 947–975.

Pedlosky, J., 1975: The development of thermal anomalies in a coupled ocean-atmosphere model. *J. Atmos. Sci.,* **32,** 1501–1514.

Pitcher, E. J., M. L. Blackmon, G. T. Bates and S. Muñoz, 1988: The effect of North Pacific sea surface temperature anomalies on the January climate of a general circulation model. *J. Atmos. Sci.,* **45,** 173–188.

Roads, J. O., 1986: Forecasts of time averages with a numerical weather prediction model. *J. Atmos. Sci.,* **43,** 871–892.

——, 1987a: Predictability in the extended range. *J. Atmos. Sci.,* **44,** 3495–3527.

——, 1987b: Lagged-average predictions in a predictability experiment. *J. Atmos. Sci.,* **45,** 147–162.

——, 1989a: Dynamical extended-range forecasts of the lower tropospheric thickness. *Mon. Wea. Rev.,* **117,** 3–28.

——, 1989b: Linear and nonlinear responses to middle latitude surface temperature anomalies. *J. Climate,* **9,** 1014–1046.

Salmon, R., and M. C. Hendershott, 1976: Large-scale air–sea interactions with a simple general circulation model. *Tellus,* **28,** 228–242.

Schubert, S. D., and M. Suarez, 1989: Dynamical predictability in a simple general circulation model: Average error growth. *J. Atmos. Sci.,* **46,** 353–370.

Shukla, J., and M. J. Fennessy, 1988: Prediction of time-mean atmospheric circulation and rainfall: Influence of Pacific sea surface temperature anomaly. *J. Atmos. Sci.,* **45,** 9–28.

Tribbia, J. J., and D. P. Baumhefner, 1988: Estimates of the predictability of low-frequency variability with a spectral general circulation model. *J. Atmos. Sci.,* **45,** 2306–2317.

World Meteorological Organization, 1988: *Modelling the Sensitivity and Variations of the Ocean-Atmosphere System,* Report of a Workshop at the European Centre for Medium-Range Weather Forecasts, WCRP-15, WMO/TD-No. 254, 294 pp.